

The Tiny Time-series Transformer: Low-latency High-throughput Classification of Astronomical Transients using Deep Model Compression

Tarek Allam Jr.,¹* Julien Peloton,² Jason D. McEwen^{1,3}

¹Mullard Space Science Laboratory, University College London, Holmbury St Mary, Dorking, Surrey RH5 6NT, UK

²Université Paris-Saclay, CNRS/IN2P3, IJCLab, 91405 Orsay, France

³The Alan Turing Institute, British Library, 96 Euston Rd, London NW1 2DB

Accepted XXX. Received YYY; in original form ZZZ

ABSTRACT

A new golden age in astronomy is upon us, dominated by data. Large astronomical surveys are broadcasting unprecedented rates of information, demanding machine learning as a critical component in modern scientific pipelines to handle the deluge of data. The upcoming Legacy Survey of Space and Time (LSST) of the Vera C. Rubin Observatory will raise the big-data bar for time-domain astronomy, with an expected 10 million alerts per-night, and generating many petabytes of data over the lifetime of the survey. Fast and efficient classification algorithms that can operate in real-time, yet robustly and accurately, are needed for time-critical events where additional resources can be sought for follow-up analyses. In order to handle such data, state-of-the-art deep learning architectures coupled with tools that leverage modern hardware accelerators are essential. We showcase how the use of modern deep compression methods can achieve a 18× reduction in model size, whilst preserving classification performance. We also show that in addition to the deep compression techniques, careful choice of file formats can improve inference latency, and thereby throughput of alerts, on the order of 8× for local processing, and 5× in a live production setting. To test this in a live setting, we deploy this optimised version of the original time-series transformer, $\tau 2$, into the community alert broking system of FINK on real Zwicky Transient Facility (ZTF) alert data, and compare throughput performance with other science modules that exist in FINK. The results shown herein emphasise the time-series transformer’s suitability for real-time classification at LSST scale, and beyond, and introduce deep model compression as a fundamental tool for improving deploy-ability and scalable inference of deep learning models for transient classification.

Key words: machine learning - software - data methods - time-series - transients - supernovae

1 INFERENCE IN THE AGE OF LARGE SYNOPTIC SURVEYS

The turn of the century has seen a move towards ever larger astronomical surveys, collecting large volumes of synoptic data across the night-sky, as opposed to previous instruments that focus data collection for a single science case. Being able to conduct a large swath of science from a single data source is one of the main drivers for development and construction of such surveys, and allows for many science communities to benefit from a single instrument. Recent surveys such the Sloan Digital Sky Survey (SDSS York et al. 2000), the Dark Energy Survey (DES Abbott et al. 2016), the Panoramic Survey Telescope and Rapid Response System (Pan-STARRS Kaiser et al. 2002) to name a few, are examples of astronomical surveys that map the sky without a particular astronomical *target* in mind. They are often limited in scope in terms of electromagnetic spectrum, but can serve as the precursor to more specialised instruments for follow-up observations. Typically, surveys are used to generate catalogues of

astronomical objects, as well as logging astronomical transient events on the sky.

The detection of transient events is of particular importance for probing the nature of dark energy and constraining theories of the Universe (Riess et al. 1998; Perlmutter et al. 1999). Typically SNe, which are observed over a period of a few days to a few weeks, are classified by the presence of particular absorption lines in their spectra. Specifically, Supernovae Type-Ia (SNIa) are distinguished by the absence of hydrogen lines and the presence of Si II λ 6150 absorption (Riess et al. 2001). However, spectroscopic classification of transient events is a costly process. By using broad photometric passbands, LSST will be able to “see” far more events than ever before, or that could be possible with spectroscopic equipment. The problem then arises: how can one accurately identify different transient photometrically using only passband information? In contrast to spectroscopic classification, photometric classification is far more challenging, and one is more susceptible to cross-contamination from other events such as core-collapse SNe (SNe Ib/c and SNe II) which share a similar profile to SNIa when observed photometrically. Consequently, studies have been done by similar photometric surveys to determine the acceptable level of cross-contamination from such

* E-mail: tarek.allam.10@ucl.ac.uk

events that would still allow for robust cosmological analysis of the dark energy equation of state. This range has been reported to be between 8% (DES [Vincenzi et al. 2021](#)) and 5% (Pan-STARRS [Kaiser et al. 2002](#)). It is expected LSST will require a high SNIa purity and cross-contamination rate to be at least within this range, if not lower. It should be noted that these levels are in the context of full phase light curves, and so one may expect a higher level of cross-contamination in the early phase of the events, where only partial information is available for identification.

When making observations photometrically, the flux measurement corresponding to a given passband is obtained by collecting all light that is received through that particular filter. Multi-band photometry allows for more information to be retrieved to help determine properties of the light source, such as temperature, but this is of course not as rich as observing spectroscopically. However, if one collects multi-band photometry over a period of time, of the same source, a light curve can be constructed, which tells us more about what kind of a transitive event this may be.

The image processing method of difference imaging measures differential photometry by matching the pointing and point-spread function(s) between image frames, typically for the detection time-varying celestial objects ([Wang et al. 2017](#)). A new image is compared with an aligned reference image, where the difference between the two images is determined by calculating the difference between each pixel of each image, and forming a difference image from the result. A detection occurs when the difference image is above a certain signal-to-noise threshold. When this threshold is reached, a transient event alert is triggered, with data streamed to brokers around the world for follow-up analysis.

With difference imaging processing now done entirely in software, the need to automate pipelines for detection and classification of transient events comes from the sheer volume of data these surveys generate, as well as the number of events they witness. Developments in instrumentation have allowed these surveys to scan larger areas of the sky and more detailed than ever before, with the consequence being that machine learning has now become a critical component in order to process the data.

When the Legacy Survey of Space and Time (LSST) at the Vera C. Rubin Observatory comes online, it is expected to observe 10 million variable and transient events per night, generating on the order of 1TB of data per night¹. The tsunami of transient alerts that is to be distributed globally, calls for machine learning systems that can scale to such data rates, and yet still provide robust identification of events. A classifier that can process an alert and provide classification scores in real-time will not only enable efficient allocation of resources for follow-up observations, but assist with labelling of the millions of events which is certainly beyond humans at this point. At this scale, storage space and computational costs becomes a real concern, and so for real-time processing and machine learning enriched catalogues to be feasible, classification modules need to be lightweight in terms of storage space and runtime memory footprint. Furthermore, computations should be done as efficiently as possible to not only save on time, but also money by minimising energy usage.

We structure this article in the following way. Section 2 discusses the challenges involved when dealing with a large influx of data from space surveys, and stresses the need for alert brokering systems. We touch on the policies in place for developing such brokers and de-

scribe what motivates the use of the Zwicky Transient Facility (ZTF [Bellm 2014](#)) alert stream in preparation for the upcoming LSST data distribution in Section 2.2. Following that, our focus turns to one broking system in particular, FINN ([Möller et al. 2021](#)), which served as the platform for the research discussed later in this article. Section 4 explains the ideas behind the engineering efforts that ultimately allowed for our deep learning model to successfully operate in a production system. Our preliminary results on local tests are showcased in Section 5, followed by the results of applying our methods in real-world conditions in Section 6. We then conclude in Section 7 with a discussion of these results, and how use of the methods described facilitate efficient deep learning and real-time inference, at LSST scale.

2 CALLING ALL BROKERS!

Due to computational constraints, and limits on bandwidth, the full distribution of alerts from LSST Data Facility² will only be sent out to a select few community brokering systems, whose primary purpose is to provide catalogue cross-match functionality and photometric classification of objects, thereby enriching the raw alert packets with value-added information for downstream scientific investigations. A worldwide call for brokering systems was announced in 2019 to entice teams interested in potentially building such systems ([Bellm et al. 2019a](#)), which was soon followed by a call for concrete proposals the following year ([Bellm et al. 2020](#)).

2.1 Community Alert Brokers

Since the full alert stream can not be accessed directly by scientists, community brokering systems are essential software systems that will enable time-domain science ([Bellm et al. 2019b](#)). Further to the requirements of cross-matching and photometric classification, brokers are also expected to provide additional services to enable science such as a simplified user interface for easy querying of archival data, a triggering follow-up observing service, additional alert filtering³, among others. The call for brokers was not limited to any institutions in particular, and the open call encouraged a variety of system designs. As long as there is capacity for petabytes (PB) of storage space, a large inbound bandwidth network, real-time machine learning classification modules, and of course sufficient funding, brokering teams were free to set out their plans in The Call for Proposals for Community Alert Brokers ([Bellm et al. 2020](#)). Naturally, brokers that offer a suite of services along with the necessary infrastructure capabilities, were seen more favourably by the selection committee, and in particular brokers that take advantage of the unique real-time aspects of the LSST alert stream ([Bellm et al. 2020](#)). Moreover, brokers that already exhibit integrations with follow-up resources and other surveys through existing agreements, as well as scope for community building, was also viewed positively.

Of the many teams that put forward proposals, seven teams were ultimately chosen that showcased their ability to match the criteria laid out above, or at least showed the potential to realise the requirements come time of first light. The successful broker bids were from teams; The Automatic Learning for the Rapid Classification of Events (ALerCE) ([Förster et al. 2021](#)), AMPEL ([Nordin et al. 2019](#)),

¹ Raw data volume for image and calibration data will not be distributed with the alerts to save space and reduce the data sent over the wire, which would otherwise amount to 60PB over the course of 10 years of operation.

² lsst.org/about/dm/facilities

³ The LSST Data Facility applies its own filtering of alert packets such as a criterion of SNR > 5 and before distribution

Arizona-NOAO Temporal Analysis and Response to Events System (ANTARES) (Matheson et al. 2021), BABAMUL (Duev & Graham 2022), Pitt-Google (Wood-Vasey et al. 2022), Lasair (Smith 2019) and FINK (Möller et al. 2021).

2.2 The ZTF Alert Stream: A Proxy for Success

In order to support development of the broking systems, LSST provided example alert streams to get broking teams familiar with the expected data formats and protocols. Much of these were inspired by the Zwicky Transient Facility (ZTF) already-in-action alert distribution system (Patterson et al. 2019). The Zwicky Transient Facility (ZTF) is an astronomical survey that observes in visible and infrared, primarily focusing on the detection of transient objects that change rapidly (Bellm 2014). Its high cadence allows it to observe the entire northern sky in three nights over two passbands⁴. Although generating only a tenth of the data expected from the LSST, the data pipelines and alert distribution systems in place with ZTF have been shown to be suitable to act as a precursor to the much larger data rates of fully operational LSST (Patterson et al. 2018).

The ZTF alert packets are in Apache Avro⁵ format, a binary serialisation format, that contains difference imaging information of the detection, yet is still compact and lightweight enough for real-time worldwide publishing. Deserialisation is done in conjunction with a corresponding alert schema that defines the contents of the alert packet, and hence the information that can be used for processing. LSST is set to follow the same data format as well as the same *pub-sub* framework using Apache Kafka⁶ for the distribution of the streaming data, where it collects data streams at source, from *producers* (e.g. the telescope itself) and arranges them into sets of *topics* that can be subscribed to by *consumers* downstream (e.g. community alerts brokers).

Since 2018, the ZTF alert production system produces on average 250 thousand new alerts nightly, and it has shown to successfully support streams of 1.2 million nightly alerts, which equates to approximately 70 GB per night, where each alert packet has been made available within 10 seconds of event detection (Patterson et al. 2018). On the order of 80,000 alerts per minute, the stability of the production system when dealing with such data rates gives support to the case for using the same technologies and protocols described in Patterson et al. (2018) for developing brokers that are to be suitable for the 10× larger upcoming Large Survey of Space and Time (larger in terms of number of alerts, but also in terms of alert size).

2.3 FINK: A Next Generation Broker

Of the seven brokers mentioned in Section 2.1 that were successful in securing a spot as one of the brokering systems, we discuss FINK in more detail here. FINK is the system that the modified deep learning model of Allam, Jr. & McEwen (2021) was deployed to, and was the ultimate test bed for investigating the real-time capabilities of the original time-series transformer (Allam, Jr. & McEwen 2021). FINK goes beyond typical brokering systems by providing real-time transient classification through fast state-of-the-art deep learning algorithms that can be re-trained at low cost in a short space of time, and by using active learning techniques, specifically online learning,

that allow for continuous self-improvement of classification scores. Specifically designed to address the challenges outlined in Section 1, it uses industry standard tools for efficient big data processing. In order to carry out nightly processing of the terabyte data stream, FINK uses fault-tolerant Apache Spark (Zaharia et al. 2016) for scaling out computations across many computers, and Spark Structured Streaming (Armbrust et al. 2018) to easily interact with Apache Kafka for *consuming* the data stream.

FINK currently has a memorandum-of-understanding (MoU) with the Zwicky Transient Facility (ZTF), allowing it to receive real alert packet data, in the form described in Section 2.2, each night. This makes FINK well suited for not only testing how well deep learning models can perform under stress with real-time constraints, but also to test how well models handle classification of *real* data. The FINK system diagram can be seen in Figure 1. Along with mapping the flow of data through the broker, Figure 1 also shows at which stage the redistribution of enriched alerts will take place. The interplay of the photometric classification modules in the Processing cluster, additional third-party survey data via the Communication cluster and aggregation of value-added information in the Storage cluster, form the foundations of the Science Portal, which can be used to enable scientific analysis and offline querying of the archival data for those in the community. As of 2023, the Science Portal gives access to more than 10 TB of alert data.

3 THE TIME-SERIES TRANSFORMER

This section reviews the time-series transformer architecture of (Allam, Jr. & McEwen 2021) that motivated this work and highlights the appeal of using such an architecture for fast and efficient astronomical transient classification.

3.1 The Motivational Driver

The problem of time-series classification is one that extends to a vast number of disciplines. As with many domains, traditional approaches involved hand-crafted feature engineering to uncover patterns that would be useful for classification. Today, with the sheer volume of data, deep learning methods are being investigated as a promising alternative to previous methods for classification (Fawaz et al. 2019).

Of the deep learning methods applied to general time-series classification discussed in Fawaz et al. (2019), the most successful architectures have been variants of convolutional neural networks (CNNs) with work by Wang et al. (2016) and by Geng & Luo (2018). In the field of astronomy, recurrent neural networks (RNNs) have become popular for astronomical transient classification (Möller & de Boissière 2020; Muthukrishna et al. 2019; Charnock & Moss 2017).

Although these deep learning methods achieve impressive results, both RNNs and CNNs often struggle when dealing with time-series data of increasing sequence length. The inherently sequential structure of RNNs makes parallelisable computation troublesome since each input point needs to be processed in order. CNNs, on the other hand parallelise easily and, with the use of the dilated convolution, larger sequences can be processed (Oord et al. 2016). Having said that, CNNs suffer greatly from being relatively computationally expensive compared to RNNs (Vaswani et al. 2017). The transformer architecture and accompanying self-attention mechanisms help mitigate these problems faced by CNNs and RNNs for long-sequence

⁴ Only *g* and *r* filter bands are available from the public alert stream, while the *i* filter band is only accessible to the private part of the survey.

⁵ github.com/apache/avro

⁶ github.com/apache/kafka

⁸ github.com/apache/hbase

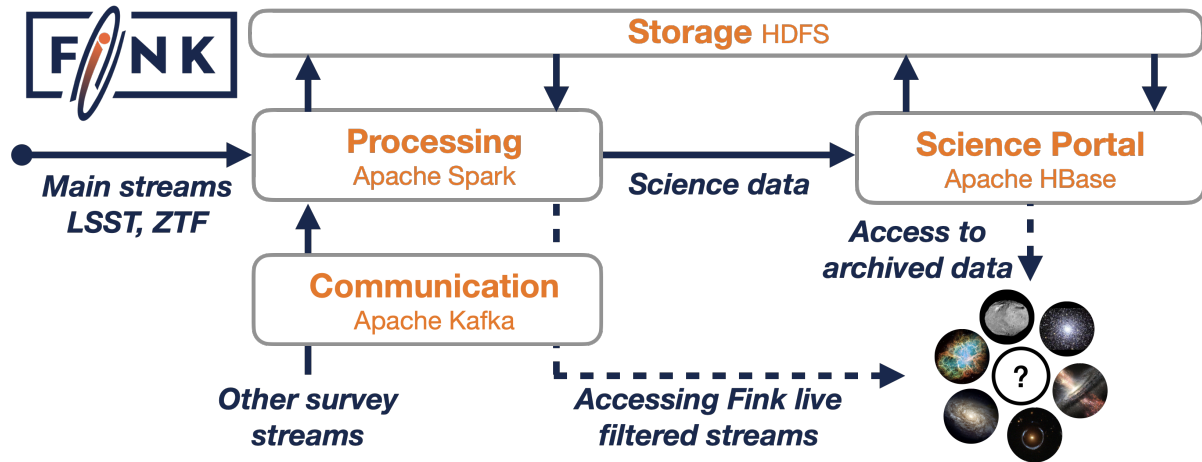


Figure 1. FINK pipeline and system architecture, where the main alert streams are processed in a distributed manner using Apache Spark (Zaharia et al. 2016) on a Processing cluster. Following the initial processing, a set of sub-streams are produced which users can subscribe to by way of the Communication cluster using Apache Kafka. Further survey data streams, such as those from LIGO, Fermi, etc. are ingested into the Processing cluster through the Communication cluster, to enrich alert packets with added information. This is used in conjunction with science modules within the Processing cluster that provide classification scores for alerts and added-value information. After a night of operation, the processed and enhanced data is written to the Hadoop Distributed File System (HDFS) in the Storage cluster which connects to a Science Portal backed by the distributed database of Apache HBase⁸ to allow for interactive querying of archived alerts. Reproduced in full from Möller et al. (2021)

time-series data (Vaswani et al. 2017). The work by Allam, Jr. & McEwen (2021) proposed a new transformer architecture for time-series classification that was originally motivated by astronomical transient classification but was found to be versatile enough to be applied to general multivariate time-series data.

As described in Allam, Jr. & McEwen (2021), the time-series transformer, t_2 , shown in Figure 2, forgoes the decoder arm of the traditional transformer architecture of Vaswani et al. (2017) yet adds new layers for Gaussian Process interpolation and inclusion of additional features. The few number of parameters used in this model compared to other deep learning approaches, combined with fast and parallelisable nature of the attention mechanisms within make for an appealing architecture to be deployed. In the next section we discuss the performance engineering choices that were made to improve the time-series transformer’s capabilities even further, placing it into the realm of production ready real-time systems operating at scale.

4 PERFORMANCE ENGINEERING FOR DEPLOYMENT IN FINK

Since photometric classifiers are to be housed in the Processing cluster (see Figure 1), low-latency, high-throughput algorithms are essential to handle the deluge of data that is to be processed. This section describes the research and development of a multistage compression process in order to ensure best classification performance, while optimising for low-latency inference and high-throughput processing of alerts.

4.1 Line Profile Analysis

In order to better understand the bottlenecks in our deep learning pipeline from alert packet processing to inference, as well as to investigate the overall systems performance, it is necessary to conduct a form of dynamic program analysis. In contrast to static program analysis, which evaluates a program without execution, dynamic program analysis focuses on the program’s memory usage, time complexity,

duration of function calls etc. Such analyses are typically done through unit and integration tests, which themselves may include, or can exist separate to the main codebase and line profiling tests that scrutinise a program line-by-line. By observing time spent at each function call, one can see where in the pipeline optimisations can be made, and as such apply performance engineering techniques that reduce runtime and memory footprint of the program.

To run such a test, we simulate locally the full pipeline from ingestion of a real ZTF alert packet, to interpolated time-series, to model predictions, and gauge where optimisations should be applied by using the line profiling tool `kernprof`⁹. The line profiling software reports the time spent on each function and the number of times that function has been called, for each line of code in a Python program.

Although initial expectations were that the main bottleneck would be the time-series interpolation through Gaussian processes, the major bottleneck in the pipeline was found to be loading our model into memory and applying the model to the input data for predictions (see Listing 1). To combat this, we looked into ways of reducing model size for faster model loading and operational changes to improve runtime latency.

Listing 1: Line profile report for initial run of alert packet pipeline. Superfluous lines that recored less than 0.1% time are removed for better readability. Note the function to generate the Gaussian process only takes 9.5% of the total time, with the majority of time taken up with model predictions. For the full report, see github.com/tallamjr/astromet/astromet/tests/reg

```
Total time: 5.85664 s
File: get_models.py
Function: get_model at line 29
```

```
Total time: 1.47076 s
File: ztf-load-run-lpa.py
Function: t2_probs at line 55
```

```
Line # Hits Time Per Hit % Time Line Contents
```

⁹ github.com/pyutils/line_profiler

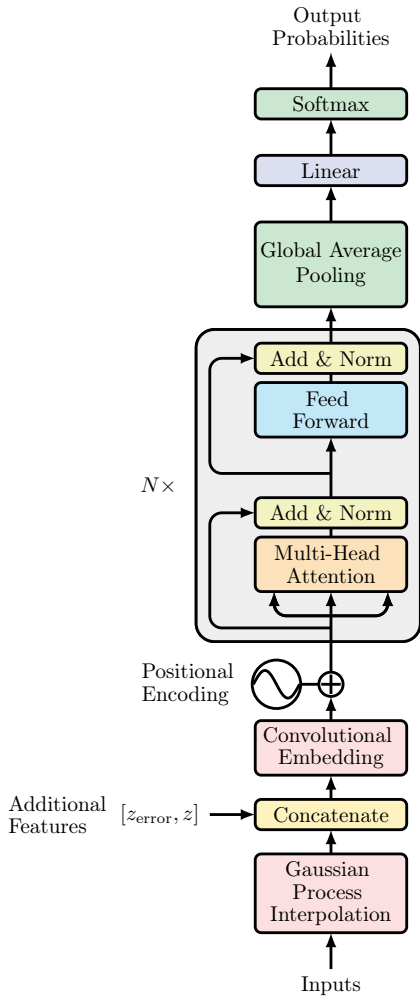


Figure 2. Schematic of the time-series transformer (t2) architecture (Allam, Jr. & McEwen 2021). If the time-series signal is irregularly sampled, then data is passed through the Gaussian process interpolation layer, followed by a concatenation layer to include any additional features. The embedding layer follows to transform the input, with a positional encoding applied to this embedding vector. The following multi head attention block is the same as that shown in Vaswani et al. (2017). A GAP layer is then applied and finally a linear layer with softmax to output class prediction probabilities for the objects. Reproduced in full from Allam, Jr. & McEwen (2021).

```

...
206 16 139.6 8.7 9.5 df_gp_mean = generate_gp_all_objects()
...
...
212 8 180.8 22.6 12.3 X = df_gp_mean[cols]
213 8 12.3 1.5 0.8 X = rs(X)
...
...
217 8 1101.7 137.7 74.9 y_preds = model.predict(X)

```

4.2 Deep Compression

With the major bottleneck for fast inference identified to be at the model load and then prediction stage, we focus our attention to model optimisations that can be applied to alleviate this. Since our desire is

to run the complex model in real-time, we look to exploit redundancies in the model, thereby reducing the storage size, lowering inference latency, and improving energy efficiency processing alerts. A relatively recent area of research that looks to reduce model size and memory footprint of deep learning models is that of *deep compression* (Han et al. 2015a). Originally proposed as a three-step process to reduce the computational cost and memory usage of deep networks on embedded devices, it is mostly driven today by the interests of industry for deploying deep learning models in-the-wild on resource constrained devices. This influential work saw a new field flourish that combines bit saving best-practises with deep learning architecture design to reduce storage size, whilst at the same time preserving model accuracy.

For our research, we restrict our investigation to the techniques broadly laid out in Han et al. (2015a), namely *weight-pruning* and *weight-clustering* with Huffman encoding, and *weight-quantization*. All of which can be applied in isolation or together, with the caveat being that if these techniques are chained together, the possibility for severe degradation in performance is high.

4.2.1 Pruning

Pruning is a technique that removes unimportant weights to yield improvements such as better generalisation and improved speed of learning and classification (LeCun et al. 1989). It has been shown in recent times that deep neural network can be pruned to a significant degree with little reduction in model accuracy (Han et al. 2015b,a).

While there are many forms of network pruning such as layer-pruning (Lazarevich et al. 2021), channel-pruning (He et al. 2017), filter-pruning (Enderich et al. 2021) and connection-pruning (Nguyen et al. 2021), we consider magnitude-based weight pruning here (Han et al. 2015a), where the weights are updated network-wide through a small number of fine-tuning epochs to zero out model weights that have a low impact on the final score, creating a sparse representation of the model. Sparse models¹⁰ can then leverage standard lossless compression algorithms for large reduction in model size, as well as faster inference through fewer parameters and hence fewer computations.

4.2.2 Clustering

Another method that promotes sparsity in the network is through weight-clustering. Also commonly referred to as weight-sharing, clustering works by grouping the weights of each layer in a model into a predefined number of clusters. The centroid values for the clusters are then shared among the weights in the given cluster. By dividing the m original number of weights in the network, $W = \{w_1, \dots, w_m\}$ into k clusters $C = \{c_1, \dots, c_k\}$, where $m \gg k$ there is a great reduction in the number of *unique* weight values in a model, which in turn allows for greater storage efficiency and high data compression potential. If we consider there to be n possible connections in the network, where each connection is represented by b bits, then a fully connected network would be represented with $n \cdot b$ bits. A clustered network on the other hand, with k clusters, requires only a cluster encoding index of $\log_2(k)$ together with the number of clusters with shared weights. This yields a compression rate, r , of

¹⁰ Stored in compressed sparse row (CSR) or Compressed Sparse Column (CSC) format gives $2a + n + 1$ numbers, where a is the number of non-zero elements, and n is the number of rows or columns, which is normally $\ll L \times M$ size of a complete matrix of all elements

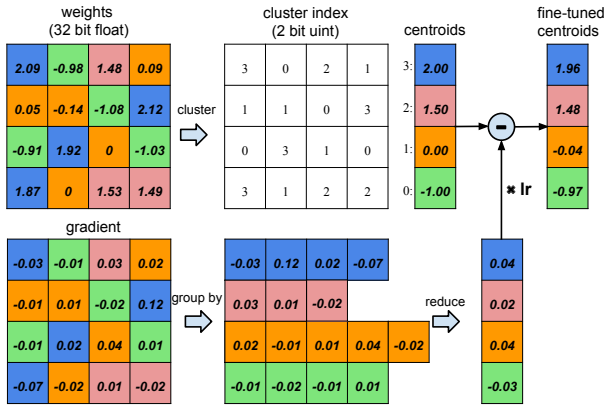


Figure 3. Weight clustering compression scheme, showing the weights of a single layer neural network that has four input and four output units. In total there are 16 weights, which are reduced to a set of 4 shared weights. The top row depicts the full weight matrix for the 4 by 4 input-output connections, whereas the bottom row shows the related gradient matrix. As an example, using 4 colours to denote the 4 clusters, the set of weights are put into one of 4 clusters, where all values in the same cluster share the same value. As such, an index mapping the weight to a particular cluster is stored. In the training phase, the gradients are grouped by colour (cluster), summed, multiplied by the learning rate, and finally subtracted from the shared centroids of the last iteration. Reproduced in full from Han et al. (2015a)

$$r = \frac{n \cdot b}{n \cdot \log_2(k) + k \cdot b} \quad (1)$$

An example using a single fully connected four-by-four neural network can be seen in Figure 3. If we use Equation 1, we can see that by setting $k = 4$ (using 4 distinct colours to signify separate clusters), one is able to reduce required number of bits for the original 16 weights at 32 bit precision, down by a notable factor with a compression rate of 3.2.

The canonical k -means clustering algorithm is used to find the clusters, but of great importance in terms of the eventual model accuracy is how the centroids are initialised. Of the three methods for centroid initialisation in Han et al. (2015a), random, density-based and linear, the authors report that random and density-based centroid initialisation achieve poor performance due to few centroids having large absolute values. Linear initialisation on the other hand does not suffer from this problem, and is shown by Han et al. (2015a) to work best under various conditions. A comparison of the different centroid initialisation schemes is shown in Figure 4. For training, a weight lookup table is necessary to maintain information about the shared weights and their connections among the clusters. The gradient for each shared weight is then calculated and used to update the actual shared weight, as can be seen in Figure 3. The gradient of the centroids is given by,

$$\frac{\partial \mathcal{L}}{\partial C_k} = \sum_{i,j} \frac{\partial \mathcal{L}}{\partial W_{ij}} \frac{\partial W_{ij}}{\partial C_k} = \sum_{i,j} \frac{\partial \mathcal{L}}{\partial W_{ij}} \mathbb{1}(I_{ij} = k) \quad (2)$$

where \mathcal{L} is the loss, C_k as the k -th centroid, and the centroid index of the weight matrix W_{ij} is I_{ij} .

At the stage for which the model is to be deployed, *i.e.* for inference operations only, the intermediate weight table can be *stripped* from the model to leave just the clustered weights, suitable for standard data compression algorithms to reduce model size on disk.

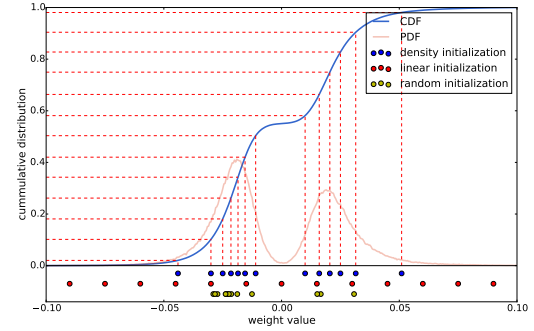


Figure 4. Centroid initialisation schemes, using the bimodal distribution of weights in CONV3 layer of AlexNet (Krizhevsky et al. 2012) as an example. Shown at the bottom are the 13 cluster centroids for this example layer using 3 different types of centroid initialisation schemes. **Random:** randomly selects k points from the data set and uses these as the initial centroids, shown in yellow. **Density:** uses the cumulative distribution of the weights to create a linear spacing on the y-axis, and then finds the corresponding x -axis value that intersects with the distribution, shown in blue. **Linear:** evenly spaces the x -axis of weights from min to max value and then places a centroid, shown in red. Random initialization tends to concentrate around the peaks of the distribution, as does density-based initialization, albeit more scattered. Linear is even more scattered, but to note the initialization scheme is invariant to the weight distribution. Reproduced in full from Han et al. (2015a)

4.2.3 Quantization

Quantization is the simple procedure of reducing the number of bits used for representing numbers. Weight-quantization helps reduce the storage and computational requirement of the model, and in the case of our discussion here, applied after training is completed¹¹. Post-training quantization refers to the application of quantization by statically mapping the weight values to lower precision integers, where in this lower precision representation, the weights save significant amount of space on disk, and can even see improvements to latency by leveraging efficient integer kernel operators found in modern hardware accelerators.

4.3 Lossless Data Compression

As touched on in our brief overview of deep compression, many of the techniques lend themselves well to exploitation by standard lossless data compression algorithms. Both pruning and clustering induce redundancies in the model through repeated values. The canonical compression scheme to handle repeated values is Huffman encoding (Huffman 1952), which assigns fewer bits to repeated values. As such, it is recommended to combine sparsity inducing methods of deep compression with lossless data compression algorithms. We use the DEFLATE algorithm (Deutsch 1996) within `zlib`¹² which combines Huffman encoding with the LZ77 compression algorithm (Ziv & Lempel 1977) to realise the full benefits of sparsifying our network. Though, we are mindful of the potential trade-off between storage space savings when using lossless compression tools and the inevitable higher latency caused by the decompression overheads when loading models into memory.

¹¹ Quantization aware training on the other hand is a quantization procedure that is applied during training by way of integer arithmetic for computations.

¹² github.com/madler/zlib

4.4 Efficient File Formats and Frameworks

While application of deep compression techniques are likely to significantly reduce the size of our deep learning model on disk, the possible increase in latency times in relation to decompression overheads spurred an off-shoot evaluation which looked at alternative file formats and lighter frameworks that could help improve runtime of model predictions.

The work of Allam, Jr. & McEwen (2021) (t2) use ProtocolBuffers¹³ as the serialisation format for saving models developed using the full TensorFlow framework (Abadi et al. 2015). Inspired by the movement (David et al. 2021), that seeks to run deep learning on *extremely* resource constrained devices, we look at the possibility of using only a subset of the full TensorFlow framework, called TensorFlow Lite (TFLite) (Li 2020). Compared to the some 1400 operations in the full framework, TFLite only has around 130 operations supported (David et al. 2021). A model developed using the lighter TFLite framework is represented in a different file format than that of the full TensorFlow model, called FlatBuffers¹⁴. This portable, efficient, binary file format offers a couple of advantages over using the ProtocolBuffers model file format, such as smaller file size through the reduced operations and code footprint, as well as much faster inference by way of zero-copy deserialisation for direct memory access without having to copy it into a separate part of memory first for an additional parsing or unpacking step.

For the most part, deep learning architectures are still designed and built using the full TensorFlow framework, and only when the practitioner is satisfied, is the model then *converted* to a TFLite model, using the helpful TFLite converter tool. The process of converting the original model to a TFLite version is where many optimisations actually take place, with the principle optimisation being operator fusion.

TensorFlow operations are themselves simple primitive operations which can be combined together to form more complex operations. The primitive operations appear as a single node in the computational graph that is constructed by TensorFlow at runtime. Composite operations that are built from multiple primitives, appear as separate nodes for each primitive operation. Fused operations, on the other hand, act as a single operation that comprises of all the computations that each primitive operation would normally have, as a single node in the graph. By taking advantage of the underlying kernel implementations, fused operations can maximize performance and reduce the code and memory footprint, perfect for the resource constrained devices that it was designed for, as well as for situations that demand low-latency inference, as in our case. A useful by-product of fused operators is a high level interface that helps define complex transformations such as quantization, that would otherwise be cumbersome to map network wide.

Under the TFLite framework, in conjunction with fused operations, quantization is far easier to achieve, and actually appears as a simple flag at conversion time when going from the original model to the TFLite version. As described in Section 4.2, quantization is the procedure of mapping floating point values to a reduced integer representation (see Figure 5), and in this TFLite setting, falls under post-training quantization umbrella. Perhaps unique to TFLite, is that at runtime, the model weights that are saved as integers, are scaled back to an approximation of the original floating point values, to allow for computations using floating point kernels to give better consistency with how inferences would have resulted had the model

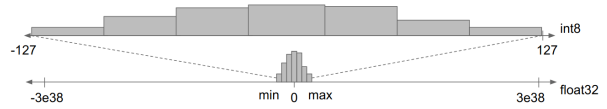


Figure 5. Quantization mapping of float representation to integers representation. With the full range for 32-bit floating points extending from $3e^{-38}$ to $3e^{38}$, there is often a remarkable amount of bits reserved for the precision, when in fact the majority of the numbers exists within a much narrow range on the number line. Integer numbers represented with 8-bits extend from -127 to 128 for signed values, and 0 to 255 for unsigned integers. With the appropriate mapping and scale factor, 32-bit numbers can be easily approximated as 8-bit integers, though 8-bit precision only has 255 information channels, this is a lossy conversion. Reproduced in full from Bhuwalka et al. (2020)

had not been quantized in the first place. The formulae for approximating floating point values from the saved integer weights can be seen here,

$$R = (Q - Z) \times S, \quad (3)$$

where the real value R is approximated by a scale factor, S , that multiplies the difference between the Q -bits representation (which is commonly taken to be 8 for 8-bit integer precision) and the zero-point value Z .

This section has described the compression schemes and optimisations applied to our deep learning model to improve latency and reduce model size, yet with the aim to preserve accuracy. Figure 6 shows where each of these techniques have been used in the time-series transformer architecture. Notably, weight-clustering has not been used architecture-wide as it is not advisable to cluster weights in critical layers early in the network¹⁵. However, as weight-pruning and weight-quantization are done post-training, we are able to apply these techniques to the model as a whole.

4.5 Hardware-Accelerated Distributed-Training

So far we have discussed optimisations that can be applied to the model in order to save on disk space and improve runtime latency such that classification scores can be given in real-time on the high-volume of incoming alerts. However, of significant importance is the ability to quickly retrain and update the model as new data becomes available. It is expected that FINK will have a window of 8 hours where new models will have the opportunity to be retrained before a new round of LSST data ingestion and processing takes place (Möller et al. 2021; Leoni, M. et al. 2022). Therefore, to have a model that can be retrained, and hence improved with more refined data, within this window is highly desirable.

As with the case in FINK, which scales out computation across many CPU-only machines in the Processing cluster to be able to churn through the large amount of data quickly, we can take advantage of the same data parallelism principles to also scale out computations for retraining models. By simply splitting the dataset across multiple compute nodes, one can achieve a near linear-time speed up. However, beyond scaling out to more CPU cores, we re-implement the time-series transformer’s training loop to scale out computations with multiple hardware accelerators, in this case graphical processing units (GPUs), for maximum speed up¹⁶. Compared to CPUs, GPUs

¹⁵ tensorflow.org/model_optimization/guide/clustering

¹⁶ We note that the codebase can easily be extended to run on even faster tensor processing units (TPUs), but this was not taken further due to lack of available resources.

¹³ github.com/protocolbuffers/protobuf

¹⁴ github.com/google/flatbuffers

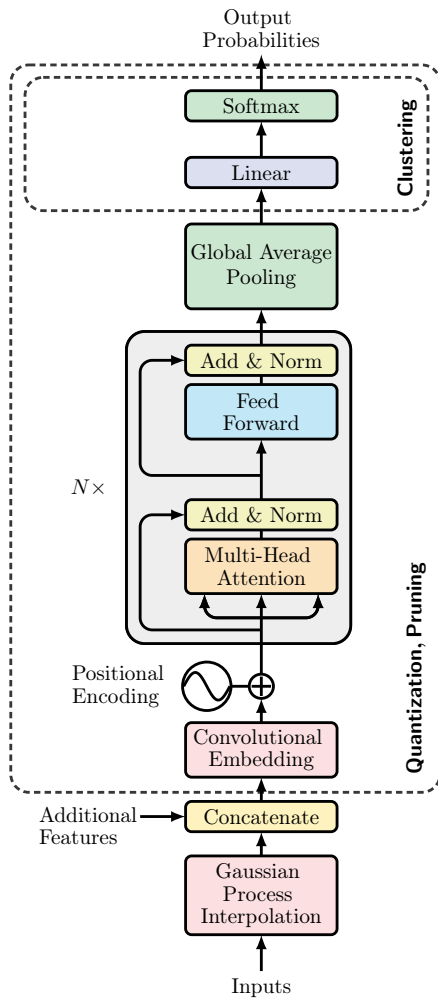


Figure 6. Locations within the time-series transformer (t2) architecture, where deep model compression techniques have been applied. We investigate three forms of model compression, weight-pruning, weight-quantization and weight-clustering. Both weight-pruning and weight-quantization techniques are applied post-training, and are applied on all weights in the network. Weight-clustering on the other hand, is applied *during* training, and only on the final dense layer to exploit parameter redundancy and to avoid the critical layers such as those in the attention block.

do computations far more efficiently, saving time, energy and costs in the long-term, but to ensure one takes full advantage of the hardware accelerators capabilities, maximising the memory use at all times is essential. If a GPU is underutilised, depending on the model and data input size, severe training time degradation can be observed due to communication overheads from host device (CPU) to the GPU accelerator. The main, and perhaps most straightforward, way one can ensure maximum utilisation is to increase data input *batch size*. It is worth clarifying here that in this setting batch size does not refer to the full dataset containing *all* training samples, rather it is a subset of training samples, equivalently called a *minibatch* (Goodfellow et al. 2016). We shall use the terms interchangeably going forward.

Batch size in itself can have a major impact on model convergence, but it plays a significant role when striving for optimal performance and computational efficiency. Since TensorFlow uses 32-bit precision for floating point operations on the GPU, model parameters take up 4 bytes each. Using this information, it is possible to determine the largest practical batch size that can deliver maximum GPU utilisation.

In addition to greater computational efficiency, larger batch sizes on the GPU are also expected to yield slight classification performance gains. If we consider that the standard error of the mean is estimated from n samples as σ/\sqrt{n} , with σ as the standard deviation of the samples, we can see that with larger n , one can obtain a more reasonable estimate for gradients (Goodfellow et al. 2016, p. 271). While it would normally be the case that the non-linear scaling of gradient estimates would invoke a trade-off between how many samples to use and compute resources, such is the computational efficiency of GPUs that the limiting factor becomes the amount of memory that can be used instead. Therefore, by increasing the batch size to be as large as possible for a single GPU, and then scaling this by the number of GPUs available, through an *all-reduce* operation when running our stochastic gradient optimisation, we can realise the improved classification performance in addition to computational improvements as well.

5 PRELIMINARY RESULTS

This section presents the preliminary results of applying the model optimisations outlined in this article to the original time-series transformer model (Allam, Jr. & McEwen 2021). We first run local processing tests on real ZTF alert packets to gauge the potential performance when deployed into the production system of FINK (which is discussed in the next section).

5.1 Model Retraining

The original time-series transformer was trained using a single NVIDIA V100 GPU, with 32GB of memory. Section 4.5 explained how computational efficiency gains could be made by increasing batch size. As a first test, we extend the t2 codebase to allow for multiple GPU training while ensuring the largest batch size possible is dispatched to each GPU. Through the model profiling tool of `model-profiler`¹⁷ we determine the best minibatch size to be 4096 using the same GPU as before. Now on the order of 100 times larger batch size compared to the original model described in Allam, Jr. & McEwen (2021), we see far greater utilisation of the GPU.

Scaling out computations across many machines and increasing the global batch size gave remarkable speed up, bringing training time down from approximately 8 minutes per epoch to 2 minutes per epoch, where epoch refers to one full forward pass and one full backward pass of all the examples in the training set. With an average convergence rate of 130 epochs, we bring overall model training down from 17 hours to nearly 5 hours, now well within FINK’s window of opportunity for retraining new models nightly. Note that this is a full model retrain, and simple fine-tuning can be done at a fraction of the time should this be the preferred method of model updating. By leveraging data parallelism in this way, where the data is distributed across multiple devices for training, should even more hardware accelerators become available, we can bring this down further still with a *near-linear* reduction in training time.

5.2 Local Processing Tests

With the knowledge that we can retrain models quickly within the specified window suitable for FINK nightly updates, we now move to our first application of deep model compression. We discussed

¹⁷ pypi.org/project/model-profiler

in Section 4.2 that of the three methods: weight-clustering, weight-pruning, and weight-quantization, only clustering is applied during training. To enable this, we modify our original model to allow for clustering of weights in the network.

Clustering, otherwise known as weight-sharing, can indeed be done throughout the network. However, it is advisable to avoid highly specialised layers such as attention blocks, and only focus clustering on the layers that are likely to have high redundancies. For this reason, we only apply clustering to the final dense layer, as shown in Figure 3.

Firstly, we inspect the impact weight-clustering alone has on the model performance compared to the original $\tau 2$ architecture. Along with application of model optimisations and compression, comes the expectation that model performance could be adversely affected. While it may be the case that the goal is to remove redundancies, by using these methods, there is inherent information loss compared to the original model, which must be considered. Under the same parameter settings and conditions as the original time-series transformer model (see Allam, Jr. & McEwen (2021), Table 2), which used the six passbands of g, r, i, z, y plus two additional features photometric redshift and photometric redshift error, we can see in Figure 7 that by using clustering, we not only preserve model accuracy, but this is improved slightly to a logarithmic-loss of 0.450 compared to 0.507 previously. This actually takes the performance beyond the previous state-of-the-art by Boone (2019) of 0.468. Furthermore, we maintain our ability to provide classifications at the level required for cosmological analysis of dark energy with a purity of 0.95 for SNIa and a core-collapse SNe (SNe Ib/c and SNe II) cross contamination of $\sim 4.5\%$, comparable to results calculated for DES (Vincenzi et al. 2021) and Pan-STARRS (Jones et al. 2018) with $\sim 8\%$ and $\sim 5\%$ respectively. However, at this point, we should note that we are potentially seeing the benefits from batch size enhancements and so slight improvements in logarithmic-loss could perhaps be attributed to this, in addition to weight clustering.

Nevertheless, redundancies have been exploited, allowing this model to achieve good classification scores at a fraction of model size on disk. With preservation of model performance confirmed, we continue to explore the impact of applying other compression methods to $\tau 2$ and inspect compression rate, inference latency and model performance trade-offs.

To continue our preliminary analysis gearing for deployment, we simulate the ingestion pipeline and use real ZTF alert packet data, such that it is akin to what the model would be expected to handle in the production system of FINK. To synthetically create a ZTF-like dataset to retrain our model, we use the same PLAsTiCC dataset (The PLAsTiCC team et al. 2018) described in Section 5.1 of Allam, Jr. & McEwen (2021), using only the time-series information *i.e.* no additional redshift features, and drop all passbands except for g and r . We then retrain to create a *new* model that can handle ZTF data, and use this as our baseline, which achieves a logarithmic-loss of 0.968. It should be noted that the synthetically generated ZTF dataset that is derived from PLAsTiCC contains full light curves. This is generally not available in real ZTF alert packet history data which only contain a candidate records for 30 days in the past. LSST on the other hand is set to provide up to 1 year of historical data per alert.

In a comparative study, we look at four main aspects when judging machine learning models for production performance: model size, model load time, model inference time, and finally model performance in terms of logarithmic-loss score. It is important to monitor any degradation in performance which would indicate whether a particular technique, or combination of techniques are still worth using. This is all shown in Table 1, which compares the baseline architecture

of the original time-series transformer described above with various compression methods and optimisations techniques applied.

The first thing to note from Table 1 is the immediate space savings one can achieve through standard lossless compression algorithms. The original model is able to be reduced down by 4.5 \times , which is significant for space savings, but it is also clear that load and inference latency are not affected. For the gains we are hoping for, deep compression methods are required, and this will be the focus of the remainder of this discussion.

The first method we apply is that of weight-clustering. We described in Figure 4 the typical ways to initialise the centroids of the clusters. We opt for using linear initialisation and set the number of clusters to be 16 for the reasons laid out in Han et al. (2015a), which puts poor performance of the other initialisation procedures down to fewer clusters containing large weight values. The immediate effects of clustering show improvements in logarithmic-loss from 0.968 to 0.836. We suspect this may be due to the reduction in the number of parameters, helping to generalise the model as alluded to in Le-Cun et al. (1989). We also see a slight reduction in model size, but considering we now have shared weights, the real model reductions are realised when we combine this with Huffman encoding, which uses fewer bits for repeated values. Hence, we see a better reduction in model size using clustering *and* Huffman encoding compared to just using Huffman encoding on the baseline model alone. We would expect far greater compression rates should the technique be applied to more layers than just the final dense layer which goes from 448 unique values to 16 values. Models which have many thousands of unique values would greatly benefit from this procedure. In addition to space saving, we also see a small reduction in load latency as well as inference latency.

We now move to the application of weight-pruning. Recall pruning removes “unimportant” weights by setting them to zero, and specifically those weights with low magnitudes. We apply this technique network wide so all layers’ weights are evaluated and trimmed down accordingly. Through fine-tuning of the clustered network, we soon discovered that any additional sparsity that was introduced negatively affected the classification scores. The results can be seen in Table 1, where even pruning to a level of 1.1% sparsity degraded performance. Further empirical studies are necessary to determine what level of sparsity would actually benefit this network. Notwithstanding, we complete our analysis by including Huffman encoding to this pruned network to witness any improvements in load time and inference latency. Indeed there is an improvement on both of these metrics, but at the cost of classification performance, we disregard using pruning any further.

We move towards a different approach for model optimisation with a change in file format and framework as described in Section 4.4, as well as application of weight-quantization. These results are denoted by the dagger (\dagger) symbol in Table 1. These are models that have originally been trained using the full TensorFlow framework but converted to a more optimised, efficient file format of FlatBuffers. The conversion also involves operator fusion, to combine primitive computations that appear as a single operation in the computational graph. With reduced code footprint through operator fusion, and efficient binary representation of data, we naturally see a large reduction in model size on disk. Around 10 \times space savings can be achieved by simply converting the original model into a TFLite model. In addition to the impressive space saving gains that are made, with the model in this format we can take advantage of directly mapping the model into memory for a reduction in load latency of more than 13,000 \times speed up compared to the exact same clustered model and almost 15,000 \times that of the original baseline. As the model is loaded

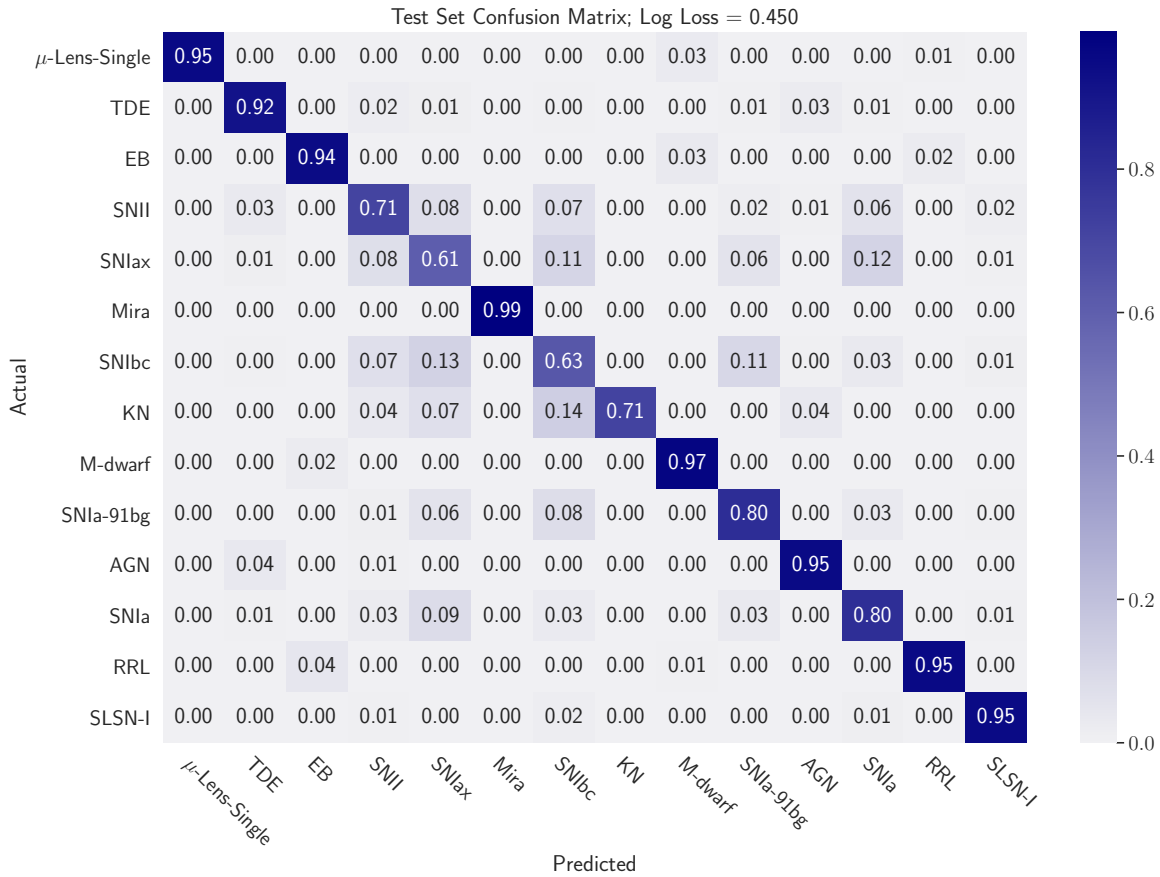


Figure 7. Confusion matrix resulting from application of a *clustered* version of the time-series transformer (Allam, Jr. & McEwen 2021), to the PLAsTiCC dataset (The PLAsTiCC team et al. 2018) in a representative setting with imbalanced classes, achieving a logarithmic-loss of 0.450, using all 6 passbands and additional information of redshift and redshift error

for each batch of data FINK processes¹⁸, this should lead to a fair increase in potential throughput of alerts. While this would certainly help with throughput of alerts in the production system, the other key metric for success is inference latency. That is, the time go from alert packet ingestion to classification. It can be seen in Table 1 using the clustered model in the FlatBuffer format gives a speed up of around 5 \times that of the same clustered model, and around 7 \times speed up compared to the original baseline. Considering our model is expected to process millions of alerts per night, having inference latency gains of this magnitude is undoubtedly positive.

Finally, we apply the third technique described in Section 4.2 of quantization. To use this method, we leverage the functionality that comes with TFLite’s model conversion tool, that allows for static quantization to 8-bit integers by examining the dynamic range of the weights when saving model to disk, and then upscaling to floating point approximation at inference time. By quantizing the weights of

the clustered model, and saving in FlatBuffer format, we are able to shrink the model even further to now 60 kilobytes, an 18 \times reduction when compared with the original baseline model, and an incredible load time improvement of 24,000 \times speed up. Moreover, inference latency is reduced slightly compared to the clustered model saved in FlatBuffer format, for an overall gain of nearly 8 \times against the baseline. An important point is to mention the preservation of model score with a logarithmic-loss of 0.834. Note the slight improvement in performance here compared to the clustered model without quantization. We suspect this discrepancy between the other clustered models to be due to the scaling approximation in Equation 3 and not due to the application of quantization itself.

We have shown that application of compression techniques and use of appropriate file formats, substantial space and memory savings, alert processing throughput, and inference latency can be achieved. However, we acknowledge local tests of the pipeline, while on real data, may not be indicative of how well a model would perform in a real production systems, under real-time constrains. Therefore, in the next section we put forward our best performing model that uses a combination of clustering and quantization to be deployed in a live setting on the production system of FINK for tests of real-time classification.

¹⁸ A batch, in this context, refers to the number of alerts bundled together to then be distributed across the cluster for processing. It is a compromise between the number alerts simultaneously processed by each mapper in the cluster, and the time delay between two alert stream polls: more alerts per mapper leads to a more efficient computation by *e.g.* minimising calls to model loading, but it will increase the time delay between two batches, leading to redistribution latencies. Therefore low latency model loading allows for more freedom when choosing batch size in FINK, and how often to poll.

Table 1. Comparative performance between the original time-series transformer model, referred as the baseline, and the respective compressed versions using a combination of weight clustering, weight pruning and Huffman encoding. We present two sets of results in terms of models saved to disk in ProtocolBuffer format and those saved in FlatBuffer format, where the latter is denoted by a † symbol. Load latency refers to the time (in milliseconds) to simply read the model into memory, whereas inference latency (in seconds) tests the time to run predictions on a single ZTF alert packet. All tests were run on an Apple M1 Pro 32GB laptop.

COMPRESSION METHOD	MODEL SIZE (KB)	LOAD LATENCY (s ⁻³)	INFERENCE LATENCY (s)	LOSS
BASILINE	1100	6324.145	0.333	0.968
BASILINE + HUFFMAN	244	6015.565	0.224	0.968
CLUSTERING	892	5559.868	0.227	0.836
CLUSTERING + PRUNING	688	5721.021	0.230	1.017
CLUSTERING + HUFFMAN	240	4991.857	0.223	0.836
CLUSTERING + PRUNING + HUFFMAN	128	5251.288	0.228	1.017
†CLUSTERING	92	0.426	0.046	0.836
†Clustering + Quantization	60	0.271	0.043	0.834

6 PRODUCTION RESULTS

In the previous section we spoke of creating a new model that can classify ZTF alert packets and hence be usable as a science module within FINK. Comparing that to the original time-series transformer of Allam, Jr. & McEwen (2021) which worked with 6 photometric passband of PLAsTiCC: u, g, r, i, z, y , as well as imputing additional features of photometric redshift, we train a model derived from the time-series transformer architecture that only takes in raw time-series from g and r bands, with no additional features. This is done to fit with the data that comes from ZTF alerts packets into FINK, which do not contain photometric redshift information but only time-series measurements for the two passbands of g and r filters. It was then this gr -only model that was used as the baseline, shown in Table 1.

Then, when using a combination of weight-clustering along with weight-quantization saved in the more efficient format of FlatBuffers, we created the best performing model in terms of latency and space saving metrics when tested locally on ZTF alert packet data. The confusion matrix in Figure 8 shows the performance of this quantized-clustered model trained on only 2 passbands. We calculate a purity of 0.89 for class SNIa, with a core-collapse SNe cross-contamination of 8%, within the expected range described for DES (Vincenzi et al. 2021) and close to the $\sim 5\%$ described in Jones et al. (2018) for Pan-STARRS.

While the model is still able to make good classification scores across the board, removing the other passbands of u, i, z cause an increase in cross-contamination by $\sim 4\%$. This is interesting in its own right, where an avenue of research could lead to investigate why training on only g and r passbands affect supernovae classification in this way compared to when we can use all 6 passbands. This may well be down to the lack of i -band specifically as this band along with r -band is typically given preference in times of good seeing and at low airmass (Abell et al. 2009), but for our purposes, we just note these results to keep in mind when assessing model validation. It should be mentioned that we only train a model of this form to suit deployment into FINK (that at the time of writing, can only ingest ZTF data), for testing of our model as a real-time classifier. It is expected for LSST that a model more akin to that showcased in Figure 7 that uses all 6 passbands as well as redshift information but trained on discretised alerts would be deployed. Efforts are currently underway to develop and deploy such a model with application to the Extended LSST Astronomical Time-series Classification Challenge (ELAsTiCC) (Naryan et al. 2022) and will feature in future work¹⁹.

This section presents the results for deploying our *quantized-*

clustered version of the time-series transformer model into the production system of FINK tested on the real ZTF alert stream. We compare the baseline model described in the previous section, that achieves 0.968 logarithmic-loss on ZTF-like data packets, with the compressed version, that achieves better logarithmic-loss of 0.834, in a now live production setting, and observe alert throughput and latency improvements that have been achieved when using the deep model compression techniques.

6.1 Model Validation

The first test for our deep learning model as a science module within FINK is to validate the classification scores that we achieve. Not only is it important for our model to operate in real-time under heavy work-load conditions, but it must clearly continue to report correct classification results when deployed. FINK validates models which target extra-galactic sources using the Transient Named Server (TNS) (Gal-Yam 2021), which is a transient alert system that has spectroscopically confirmed objects in its database. By comparing predictions to that of what TNS lists for a given object, we can get an indication of how well a transient classifier is performing.

Figure 9 shows our models predictive performance on one full year of real ZTF alerts against the spectroscopically confirmed objects in the TNS database (extra-galactic objects). In addition to the quality cuts common for all modules, we apply further criterion of at least 2 points and at most 90 points on the light curve since the first alert emission date, as well as the object to not be a Solar System object from the Minor Planet Center (MPC) database or Galactic object according to the SIMBAD database (Wenger et al. 2000). Recall in 5.2 our baseline model has been trained using full light curves. Since real ZTF alert packets contain only 30 days history, only partial light curves are observable most of the time. This results in a model being trained in non-representative setting where it expects full light curves but is tested on discretised light curves. Yet, our model is able to correctly identify the majority of SNIa objects, as well as other classes. Though it should be noted there is greater misclassification of SNIa and core-collapse SNe beyond the predicted cross-contamination of $\sim 8\%$ described above and this is likely due to the non-representative nature of the training data the model has been built upon. As such, we would not consider our model in this form to be suitable for a fine-grain transient classifier, and ideally would need to be trained on the discretised data of alert packets to be more representative, which is planned for future work. Considering these results, we can instead frame our model as to be a general transient classifier that is able to identify SNe more broadly. Indeed, when we evaluate the model against the ensemble of predictions from all other

¹⁹ portal.nersc.gov/cfs/lst/DESC_TD_PUBLIC/ELASTICC/

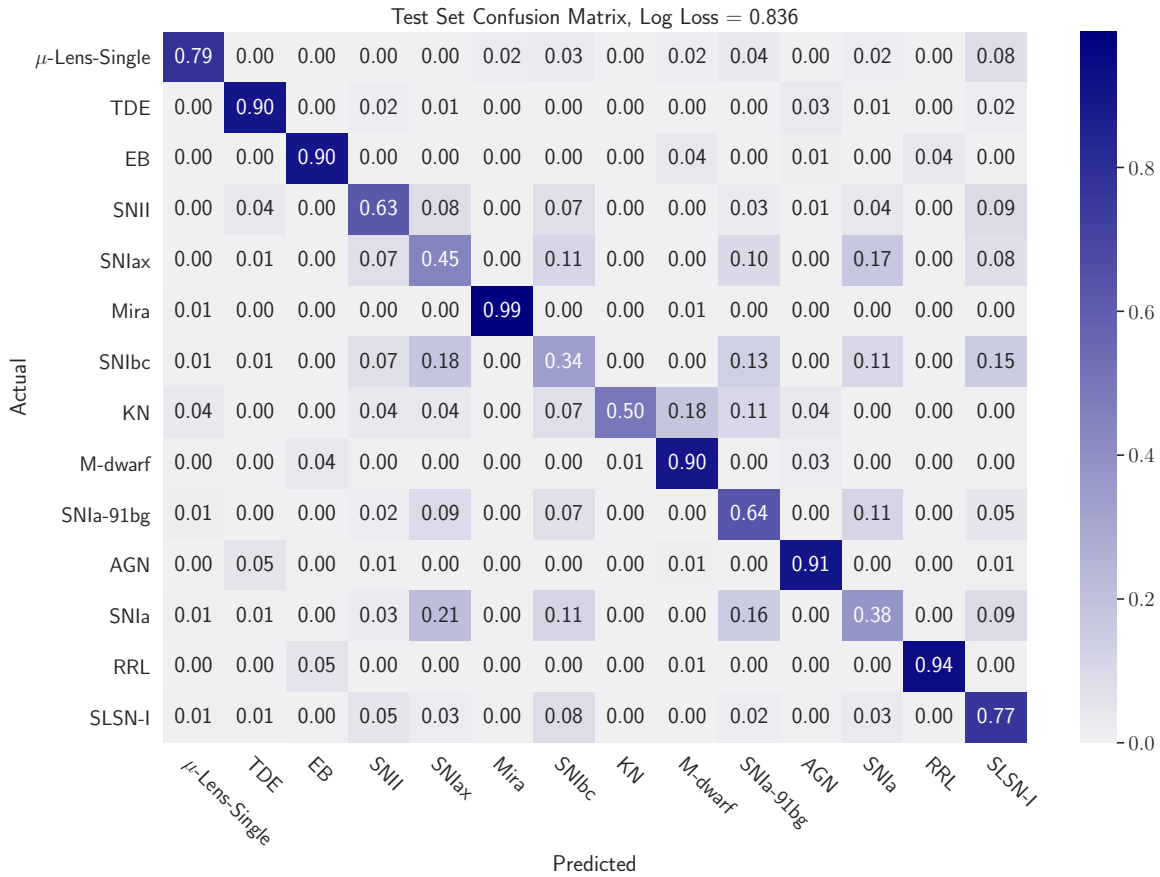


Figure 8. Confusion matrix resulting from application of a *clustered* version of the time-series transformer (Allam, Jr. & McEwen 2021), to the PLAsTiCC dataset in a representative setting using full light curves, with imbalanced classes, and only time-series information from g and r passband filters. This model achieves a logarithmic-loss of 0.836, using only the 2 passbands and no additional information.

classifiers in FINK we can see our model is able to correctly identify SN candidates, shown in Figure 10.

Therefore, while there are some misclassification within SNe classes, the compressed time-series transformer is able to successfully classify supernova objects in general, and when compared to existing science modules in FINK, correctly identifies supernova candidates. It is also able to go further, where FINK science modules labels certain objects as “Unknown”, our model is able to accurately suggest these as supernovae *candidates* (see Figure 10). A clear value-add for the brokering system which can be used to update and enrich the database.

6.2 Alert Throughput/Latency Performance

With confirmation that the compressed model is operating correctly, we now come to test the throughput and latency of the classifier, ultimately deciding the usefulness of our model for real-time classifications.

We first look at how the original time-series transformer, which we refer to as the baseline model in Table 1, fairs up against other existing science modules in FINK. For this, we take one full nights worth of ZTF alerts, amounting to approximately 200,000 alert packets, and compare the throughput and latency performances of all the science modules currently implemented in `fink-science`²⁰ as of v2.0.0. For an overall comparison, we show the “on-sky” throughput per-

formance that passes all alerts through all science modules, ignoring any pre-processing filters that would normally be applied.

Over an average of 20 processing runs, the mean alerts per second per core for each science module is calculated. These results are most succinctly presented in Figure 11, where our model is the only deep learning model of such complexity offering up a vector of probabilities for the classification scores. Other science modules such as Solar-System Object (SSO) and The Centre de Donnés astronomiques de Strasbourg (CDS) cross-matching service are examples of table lookups whose performance is determined by the execution of a query plan, and the only other deep learning model of SuperNNova (SNN) (Möller & de Boissière 2020) offers only a binary classification for SNIa.

The baseline model, with no compression or optimisations made, is actually able to sit amongst the other science modules and deliver real-time classifications. While this seems to have already achieved our desired goal of deploying a science module capable of real-time classification, it is important to consider that the model that is deployed in FINK is not done so in isolation, but rather all science modules within FINK will be operating in tandem. Correspondingly, since the outgoing enriched alert packet is only sent after *all* science modules have finished processing the data packet, each individual

²⁰ github.com/astrolabsoftware/fink-science

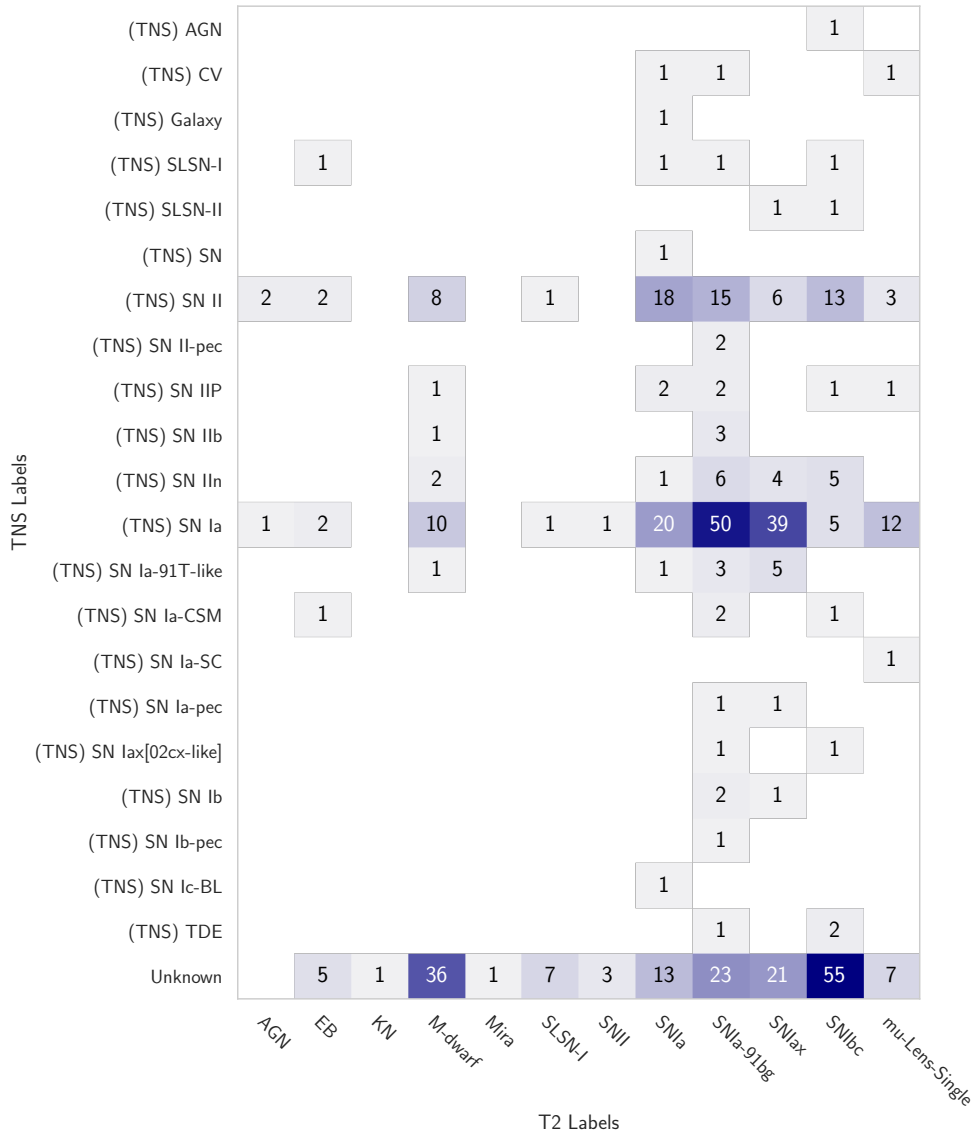


Figure 9. Comparison of spectroscopically confirmed labels in the Transient Named Server (TNS) database against the top-1 predictions for the compressed time-series transformer. The data used for this test comprised of one full year (2022) of real ZTF data with specific quality applied to the light curve history data requiring a minimum of 2 points and maximum of 90 points on the light curve since the first alert emission date. The set of alerts are also reduced to filter out objects known to be a Solar System object from the MPC database or Galactic object when cross-matched against the SIMBAD database.

science module can have a large impact on the real-time science capability of FINK as a whole. To not delay other modules that may be time-critical such as for Gamma Ray Burst (GRB) detections, science modules need to optimise throughput wherever possible, ultimately benefiting the entire system.

Therefore, by going further and looking at how our best performing compressed model manages to deal with the alert throughput in a live setting, we can see in Figure 11 a sizeable improvement. While our local processing tests gave up to 8x speed up compared to the baseline model for inference latency, in a real production environment, we achieve an impressive 5x in a live setting. It is suspected that a decline in speed up compared to what was achieved in a local processing context can be attributed to communication overheads in the cluster, where networking bandwidth becomes the bottleneck in place of computations, as well as differences in hardware capabilities.

This substantial throughput performance, thanks to low-latency inference via deep compression techniques, greatly benefits the overall FINK system. As science modules are run serially in FINK, our models ability to quickly complete processing not only ensures there is no delay to other time-critical science modules, but also permits more science modules to co-exist within the total computational time budget afforded to FINK. Finally, by improving latency in this way, we lay out a guide for other existing deep learning models, and those under current development, for how to use model optimisations for improved performance.

7 CONCLUSIONS

We have shown through deep model compression, complex models such as the time-series transformer can be made super-lightweight

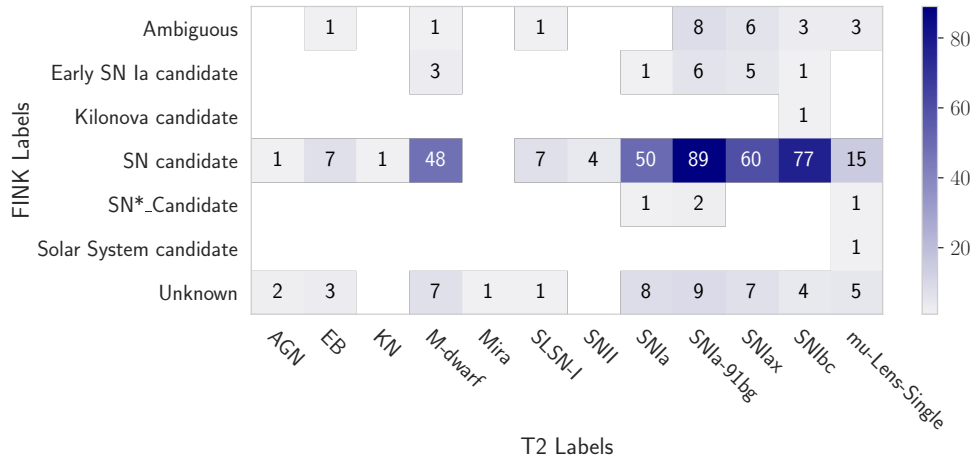


Figure 10. Comparison of aggregated FINK classifiers’ predictions against the top-1 predictions from the compression time-series transformer. One full year (2022) of real ZTF alert data is filtered according to the respective classifiers quality cuts as well as the criteria for a minimum of 2 points and maximum of 90 points on the light curve since the first alert emission date. We also ensure to disregard alerts that correspond to be a Solar System object from the MPC database or Galactic object when referenced against the SIMBAD database.

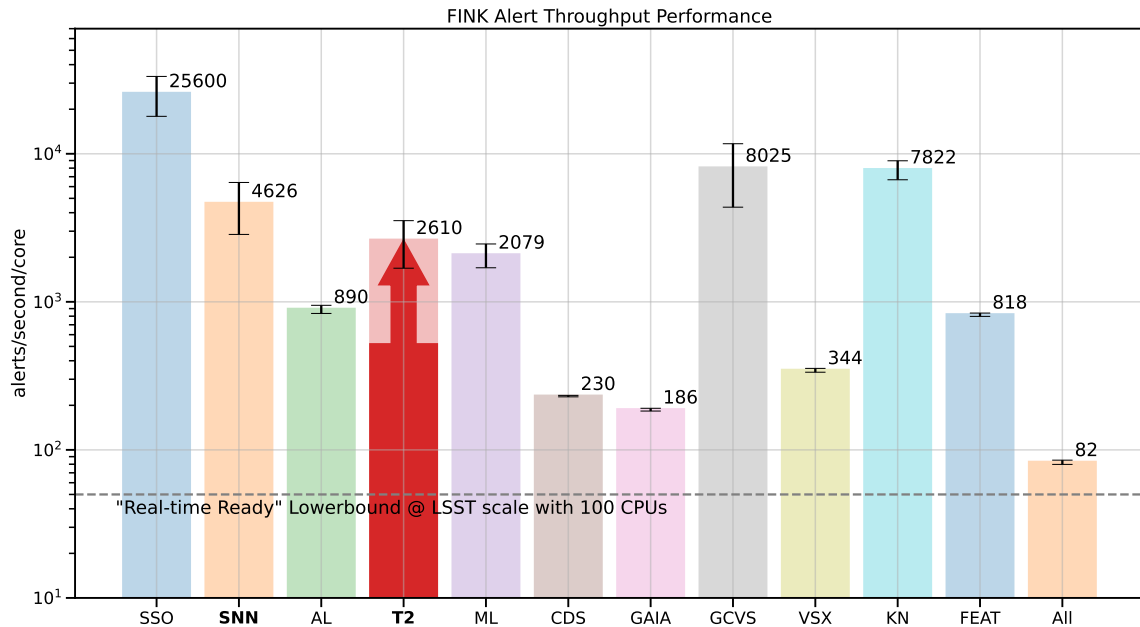


Figure 11. Alert throughput of FINK science modules, as of version `fink-science-v2.0.0`, tested on one full nights worth of ZTF alerts (approximately 200,000). As described in Möller et al. (2021), we trace a horizontal line to indicate the threshold for a single science module within FINK to be considered *real-time ready*, assuming 100 CPU cores. Under the data rates estimated for LSST, FINK will receive 10,000 alerts every 37 seconds, and such a threshold would allow for approximately a dozen science modules to provide classification scores serially. For full details of the inner workings of the other science modules shown here, the reader is advised to explore the `fink-science` package. It should be noted that the results presented here are to be considered “on-sky” performance, where all alerts are processed blindly by all modules. This would not be the case typically, for example only a small fraction of alerts would be processed by the ML (microlensing) (Godines et al. 2019) module since various inbuilt physics filters would determine if an alert is suitable for processing beforehand. Our time-series transformer model (T2), is originally able to achieve a throughput of ~ 500 alerts per second per core, but following application of deep compression techniques achieves an increased throughput of approximately 5x of the number of alerts to now ~ 2600 alerts per second per core. In this same plot we have shown the baseline performance, and the new compressed version of the time-series transformer architecture using an arrow to indicate the increase in throughput. This version of the time-series transformer that uses weight-clustering and weight-quantization along with TFLite fused operations achieves performance far beyond the requirements for real-time classification of alerts at LSST scale. This has knock-on benefits for all other science modules within FINK, and encourages use of these methods for other science modules going forward. We highlight in bold along with T2 the only other deep learning model of SNN (SuperNNova) (Möller & de Boissière 2020). The increase in throughput performance brings it within the same order-of-magnitude of alerts able to be processed, yet we are able to provide a probabilities score across all classes as opposed to a single binary classification.

for real-time inference. The already efficient architecture benefits even further from weight-clustering and weight-quantization to provide low-latency, high-throughput classification scores, all the while preserving the accuracy of the results. Our study of weight-pruning showed good reduction in model size but proved to be detrimental to performance. Clearly even the low magnitude weights of the network carry information critical for good classification.

We have shown through careful choice of file formats, major speed ups can be achieved, which in turn dramatically improves a deep learning model's ability to process inputs and operate in real-time, in a live production setting. Our compressed version of the time-series transformer now resides in FINK as one of the deployed science modules, operating at production scale providing nightly classifications for the incoming ZTF alert stream since January 2023. We have showcased our models suitability for providing robust classifications at a fraction of the original model size and runtime. By scaling out computations, we have brought retraining down to within the time frame required for nightly updating on new alert data.

As described in Section 2.2, the ZTF alerts stream, although $1/10^{\text{th}}$ of the expected LSST data rates, is a good precursor for modelling the suitability of models and infrastructure to how well they will handle future data streams. Consequently, we used FINK to emphasise our model's ability to handle such large volumes of data and have presented results that showcase its ability to cope with LSST scale, and beyond.

It is hoped that the work here, which introduces deep compression to the field of real-time transient classifiers, will be harnessed to enable existing architectures to be deployed as real-time classifiers easily into other brokering systems, as well as to inspire those currently being developed that real-time capability is within reach if techniques like those described here are applied.

ACKNOWLEDGEMENTS

The authors acknowledge the use of the UCL Myriad High Performance Computing Facility (Myriad@UCL), and associated support services, in the completion of this work. The work was also supported by the Science and Technology Facilities Council (STFC) Centre for Doctoral Training in Data Intensive Science at UCL. This work made use of the FINK community broker resources. FINK is supported by LSST-France and CNRS/IN2P3. TA would like to thank the FINK team for their helpful discussions.

DATA AVAILABILITY

All data referenced here can be found freely available online. For the original PLAsTiCC dataset, the reader is advised to explore details laid out in [The PLAsTiCC team et al. \(2018\)](#) and [Team & Modelers \(2019\)](#). Code to reproduce the work found herein can be found at github.com/tallamjr/astromet/tinno.

REFERENCES

- Abadi M., et al., 2015, TensorFlow: Large-Scale Machine Learning on Heterogeneous Systems, <https://www.tensorflow.org/>
- Abbott T., et al., 2016, Monthly Notices of the Royal Astronomical Society, 460, 1270
- Abell P. A., et al., 2009, arXiv preprint arXiv:0912.0201
- Allam, Jr. T., McEwen J. D., 2021, arXiv preprint arXiv:2105.06178
- Armbrust M., et al., 2018, in Proceedings of the 2018 International Conference on Management of Data. pp 601–613
- Bellm E., 2014, in The Third Hot-wiring the Transient Universe Workshop.
- Bellm E., et al., 2019b, LDM-612, Plans and Policies for LSST Alert Distribution, <https://ls.st/ldm-612>
- Bellm E., Blum R., Graham M., Guy L., Ivezić Z., O'Mullane W., Swinbank J., 2019a, LDM-682, Call for Letters of Intent for Community Alert Brokers, <https://ls.st/ldm-682>
- Bellm E., et al., 2020, LDM-723, Call for Proposals for Community Alert Brokers, <https://ls.st/ldm-723>
- Bhuwarka P., et al., 2020, Quantization Aware Training with TensorFlow Model Optimization Toolkit - Performance with Accuracy, <https://blog.tensorflow.org/2020/04/quantization-aware-training-with-tensorflow-model-optimization-toolkit.html>
- Boone K., 2019, The Astronomical Journal, 158, 257
- Charnock T., Moss A., 2017, The Astrophysical Journal Letters, 837, L28
- David R., et al., 2021, Proceedings of Machine Learning and Systems, 3, 800
- Deutsch P., 1996, Rfc1951: Deflate compressed data format specification version 1.3
- Duev D., Graham M., 2022, BABAMUL, <https://github.com/babamul/babamul>
- Enderich L., Timm F., Burgard W., 2021, in Proceedings of the IEEE/CVF Winter Conference on Applications of Computer Vision. pp 2596–2605
- Fawaz H. I., Forestier G., Weber J., Idoumghar L., Muller P.-A., 2019, Data Mining and Knowledge Discovery, 33, 917
- Förster F., et al., 2021, The Astronomical Journal, 161, 242
- Gal-Yam A., 2021, Bulletin of the AAS, 53
- Geng Y., Luo X., 2018, arXiv preprint arXiv:1801.04396
- Godines D., Bachelet E., Narayan G., Street R., 2019, Astronomy and Computing, 28, 100298
- Goodfellow I., Bengio Y., Courville A., 2016, Deep Learning. MIT Press
- Han S., Mao H., Dally W. J., 2015a, International Conference on Learning Representations (ICLR)
- Han S., Pool J., Tran J., Dally W., 2015b, Advances in neural information processing systems, 28
- He Y., Zhang X., Sun J., 2017, in Proceedings of the IEEE international conference on computer vision. pp 1389–1397
- Huffman D. A., 1952, Proceedings of the IRE, 40, 1098
- Jones D., et al., 2018, The Astrophysical Journal, 857, 51
- Kaiser N., et al., 2002, in Survey and Other Telescope Technologies and Discoveries. pp 154–164
- Krizhevsky A., Sutskever I., Hinton G. E., 2012, Advances in neural information processing systems, 25
- Lazarevich I., Kozlov A., Malinin N., 2021, in Proceedings of the IEEE/CVF International Conference on Computer Vision. pp 798–805
- LeCun Y., Denker J., Solla S., 1989, Advances in neural information processing systems, 2
- Leoni, M. Ishida, E. E. O. Peloton, J. Möller, A. 2022, *A&A*, 663, A13
- Li S., 2020, J. Comput. Res. Dev, 57, 1839
- Matheson T., et al., 2021, The Astronomical Journal, 161, 107
- Möller A., de Boissière T., 2020, Monthly Notices of the Royal Astronomical Society, 491, 4277
- Möller A., et al., 2021, Monthly Notices of the Royal Astronomical Society, 501, 3272
- Muthukrishna D., Narayan G., Mandel K. S., Biswas R., Hložek R., 2019, Publications of the Astronomical Society of the Pacific, 131, 118002
- Naryan G., et al., 2022, The DESC ELAsTiCC Challenge, https://portal.nersc.gov/cfs/lsst/DESC_TD_PUBLIC/ELASTICC/
- Nguyen T. N., Veeravalli B., Fong X., 2021, in International Conference on Neuromorphic Systems 2021. pp 1–8
- Nordin J., et al., 2019, Astronomy & Astrophysics, 631, A147
- Oord A. v. d., et al., 2016, arXiv preprint arXiv:1609.03499
- Patterson M. T., et al., 2018, Publications of the Astronomical Society of the Pacific, 131, 018001
- Patterson M., Bellm E., Swinbank J., 2019, h-093: Design of the LSST Alert Distribution System, <https://dmtn-093.lsst.io/>
- Perlmutter S., et al., 1999, The Astrophysical Journal, 517, 565

- Riess A. G., et al., 1998, *The Astronomical Journal*, 116, 1009
- Riess A. G., et al., 2001, *The Astrophysical Journal*, 560, 49
- Smith K., 2019, *The Extragalactic Explosive Universe: the New Era of Transient Surveys and Data-Driven Discovery*, p. 51
- Team P., Modelers P., 2019, *Unblinded Data for PLAsTiCC Classification Challenge*, doi: 10.5281/zenodo.2539456
- The PLAsTiCC team et al., 2018, arXiv preprint arXiv:1810.00001
- Vaswani A., Shazeer N., Parmar N., Uszkoreit J., Jones L., Gomez A. N., Kaiser L., Polosukhin I., 2017, arXiv preprint arXiv:1706.03762
- Vincenzi M., et al., 2021, *Monthly Notices of the Royal Astronomical Society*, 505, 2819
- Wang Z., Yan W., Oates T., 2016, *A Strong Baseline*. CoRR abs/1611.06455
- Wang D., Hogg D. W., Foreman-Mackey D., Schölkopf B., 2017, arXiv preprint arXiv:1710.02428
- Wenger M., et al., 2000, *Astronomy and Astrophysics Supplement Series*, 143, 9
- Wood-Vasey M., Daher C. M., Perrefort D., Raen T., 2022, *Pitt-Google Broker*, <https://github.com/mwvgroup/Pitt-Google-Broker>
- York D. G., et al., 2000, *The Astronomical Journal*, 120, 1579
- Zaharia M., et al., 2016, *Communications of the ACM*, 59, 56
- Ziv J., Lempel A., 1977, *IEEE Transactions on information theory*, 23, 337

This paper has been typeset from a $\text{\TeX}/\text{\LaTeX}$ file prepared by the author.